MATERIALS SCIENCE

Van der Waals epitaxy of nearly single-crystalline nitride films on amorphous graphene-glass wafer

Fang Ren[1,2†], Bingyao Liu[3,4,5,6†], Zhaolong Chen[4,6], Yue Yin[1,2], Jingyu Sun[6,7], Shuo Zhang[1,2], Bei Jiang[4], Bingzhi Liu[4,6,7], Zhetong Liu[3,4,5,6], Jianwei Wang[8], Meng Liang[1,2], Guodong Yuan[9,2], Jianchang Yan[1,2], Tongbo Wei[1,2], Xiaoyan Yi[1,2], Junxi Wang[1,2], Yong Zhang[10], Jinmin Li[1,2], Peng Gao[3,5,6,11]*, Zhongfan Liu[4,6]*, Zhiqiang Liu[1,2]*

Van der Waals epitaxy provides a fertile playground for the monolithic integration of various materials for advanced electronics and optoelectronics. Here, a previously unidentified nanorod-assisted van der Waals epitaxy is developed and nearly single-crystalline GaN films are first grown on amorphous silica glass substrates using a graphene interfacial layer. The epitaxial GaN-based light-emitting diode structures, with a record internal quantum efficiency, can be readily lifted off, becoming large-size flexible devices. Without the effects of the potential field from a single-crystalline substrate, we expect this approach to be equally applicable for high-quality growth of nitrides on arbitrary substrates. Our work provides a revolutionary technology for the growth of high-quality semiconductors, thus enabling the hetero-integration of highly mismatched material systems.

INTRODUCTION

Semiconductor van der Waals epitaxy (vdWE) has the potential to revolutionize future electronics and photonics by providing a novel material integration method (*1*–*4*). Substantial processes have been reported on the epitaxy of semiconductors on graphene (Gr)–covered single-crystalline substrates, such as sapphire (*5*–*10*), silicon (*11*–*14*), and SiC (*15*–*18*). However, in principle, this growth mechanism is remote heteroepitaxy (*19*), in which the epitaxy layer still inherits the crystallinity from the single-crystalline substrate, with strong substrate selectivity. The growth of nitrides on amorphous substrates such as transparent and large-scale glass, by contrast, is an ideal platform to explore semiconductor vdWE on arbitrary substrates, which is prospective to realize large-scale flexible electronics (*20*). Furthermore, it would broaden the concept of semiconductor heteroepitaxy and provide a simplified pathway for the hetero-integration of various semiconductors for advanced electronics and photonics.

However, such a growth method is still challenging owing to the lack of epitaxial interactions between the amorphous substrates and materials to be deposited. Until now, no successful research activity has been explored in high-quality nitride films on amorphous substrates. Various new buffer layer strategies have been considered to guide the lattice arrangement of nitride nucleation on amorphous substrates. For example, Ti interlayer was used for the growth of GaN pyramids (*21*–*23*). Besides, several efforts have been made on Gr-buffered nitride growth on amorphous substrates, such as GaN/AlGaN nanocolumns on amorphous glass substrates (*24*, *25*) and sputtered InGaN-based light-emitting diodes (LEDs) on amorphous SiO_2 substrates (*26*). However, these earlier attempts have not achieved a flat coalescence crystalline layer mainly due to the lack of controlled in-plane orientation.

In this work, we report the growth of GaN films on amorphous silica glass substrates by using nanorod-assisted vdWE, which shows much improved quality compared with previous results (*21*, *27*–*30*). The as-obtained GaN films exhibit the nearly single-crystalline characteristic; i.e., it has a single out-of-plane orientation and three in-plane orientations. The blue LED fabricated on such a GaN film shows a record internal quantum efficiency (IQE) of 48.67%. Furthermore, a flexible inorganic light-emitting device is demonstrated benefiting from the weak interfacial interaction. This work not only experimentally validates the growth of crystalline nitrides on amorphous substrates but also provides a promising route to the monolithic integration of semiconductors for advanced electronics and photonics.

RESULTS AND DISCUSSION

The nanorod-assisted vdWE method is proposed as schematically shown in Fig. 1 (A to F). First, we use Gr to realize aligned nitride nucleation islands, which inherit the crystallinity from the Gr lattice. At the second step, nitride nucleation islands absorb adatoms on the Gr surface and evolve into nanorods with aligned *c*-axis orientation and optimized in-plane orientations, which act as a good template for thermal mismatch alleviation and subsequent coalescence, aiming to the formation of a smooth nitride film.

Scanning electron microscopy (SEM) image and Raman characterization of Gr transferred on glass show that the Gr is uniform and continuous (fig. S1A and S2). Raman spectra and Raman mappings of Gr before and after metal organic chemical vapor

[1]Research and Development Center for Semiconductor Lighting Technology, Institute of Semiconductors, Chinese Academy of Sciences, Beijing 100083, China. [2]Center of Materials Science and Optoelectronics Engineering, University of Chinese Academy of Sciences, Beijing 100049, China. [3]Electron Microscopy Laboratory, and International Center for Quantum Materials, School of Physics, Peking University, Beijing 100871, China. [4]Center for Nanochemistry (CNC), Beijing Science and Engineering Center for Nanocarbons, Beijing National Laboratory for Molecular Sciences, College of Chemistry and Molecular Engineering, Peking University, Beijing 100871, China. [5]Academy for Advanced Interdisciplinary Studies, Peking University, Beijing 100871, China. [6]Beijing Graphene Institute (BGI), Beijing 100095, China. [7]College of Energy, Soochow Institute for Energy and Materials Innovations, Jiangsu Provincial Key Laboratory for Advanced Carbon Materials and Wearable Energy Technologies, Soochow University, Suzhou 215006, China. [8]School of Materials and Energy, University of Electronic Science and Technology of China, Chengdu 610054, China. [9]State Key Laboratory for Superlattices and Microstructures, Institute of Semiconductors, Chinese Academy of Sciences, Beijing 100083, China. [10]Department of Electrical and Computer Engineering, The University of North Carolina at Charlotte, Charlotte, NC 28223, USA. [11]Collaborative Innovation Center of Quantum Matter, Beijing 100871, China.
*Corresponding author. Email: lzq@semi.ac.cn (Zhiqiang Liu); p-gao@pku.edu.cn (P.G.); zfliu@pku.edu.cn (Zhongfan Liu)
†These authors contributed equally to this work.

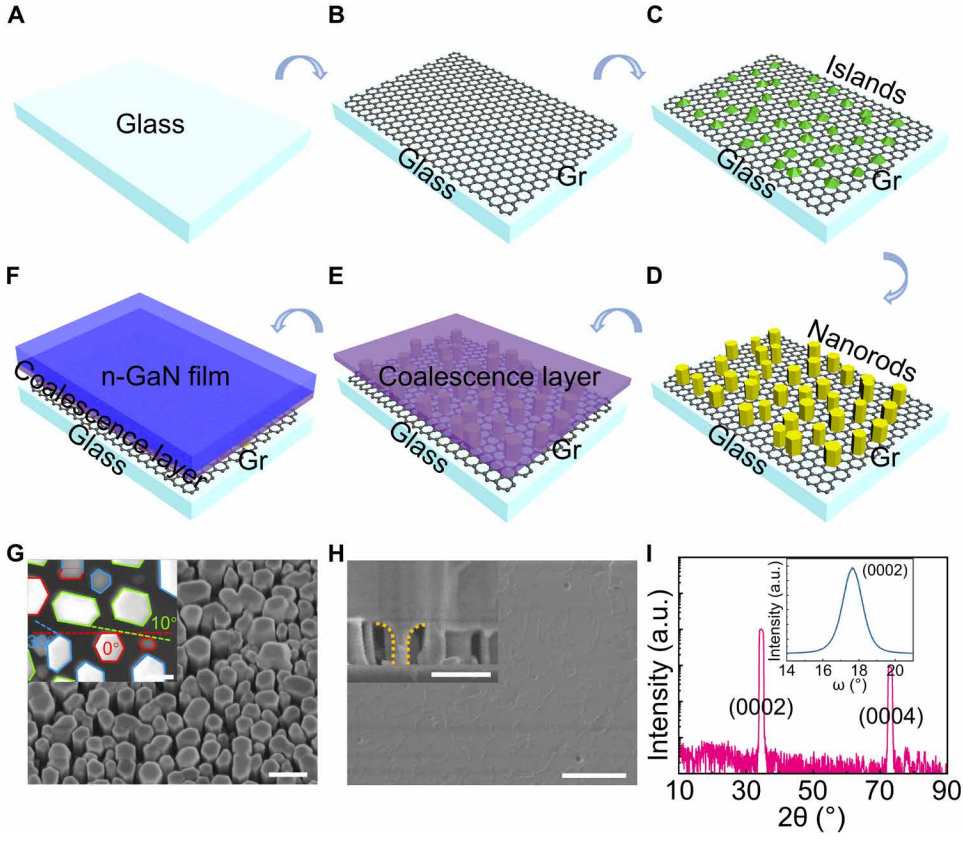

Fig. 1. The growth of GaN films on Gr/glass. (**A**) The amorphous glass substrate. (**B**) Transfer of Gr onto a glass substrate. (**C**) Nucleation islands on the Gr/glass substrate. (**D**) Growth of vertically aligned nanorods on the Gr/glass substrate. (**E**) Coalescence layer of nanorods through the ELOG process. (**F**) Continuous and flat n-GaN films atop bridging nanorods on the Gr/glass substrate. (**G**) The 25° tilted-view SEM image of vertically aligned nanorods with uniform height; the inset shows the high-magnification SEM image of hexagonal-shaped nanorods between which the relative rotation angles of about 0°, 10°, and 30° are labeled by red, green and blue lines, respectively. (**H**) The SEM image of a continuous and planar GaN film; the inset shows the ELOG process labeled by orange dotted lines. (**I**) XRD 2θ scan spectrum showing that GaN film has a wurtzite structure; the inset shows the x-ray rocking curve of (0002) for GaN films with an FWHM of 1.2°. Scale bars, 5 μm (H), 0.5 μm (G, inset of H), and 0.2 μm (inset of G). a.u., arbitrary units.

deposition (MOCVD) growth show the existence of Gr and compressive strain in Gr after GaN growth (fig. S1B and S3). The SEM image in Fig. 1G shows that the *c* axis–oriented nanorods are vertically aligned with good uniformity in height and diameter. The inset of Fig. 1G is a high-magnification SEM image of hexagonal nanorods, in which there are three in-plane orientations with relative rotation angles of approximately 0°, 10°, and 30° about the *c* axis (labeled by red, green, and blue lines, respectively). It will be discussed in detail below. After coalescence, the GaN film exhibits a continuous and flat surface (Fig. 1H and fig. S4A). As a comparison, GaN layer directly grown on the bare glass substrate, by either nanorod template or conventional low-temperature (LT) buffer method, exhibits a rough polycrystalline surface morphology consisting of random *c*-axis orientations (fig. S5, A and B). The detailed description of the control experiments is shown in Materials and Methods. On Gr-covered glass, although the *c*-axis alignment remains, the in-plane orientations are numerous because of the conventional LT buffer method (fig. S5C), hindering the formation of a continuous film. In contrast, only three dominant in-plane orientations exist by introducing the nanorod template on Gr/glass (the inset of Fig. 1G). Therefore, it is reasonable to conclude that a Gr buffer layer can well guide the lattice arrangement at the nitride/Gr heterointerface, especially in the *c*-axis direction. Significantly, the designed nanorod template further restricts the in-plane alignment to only three dominant configurations. In this case, Ga or Al adatoms at the Gr surface tend to diffuse and incorporate into nitride nanorods through lateral surface migration (fig. S6), which is energetically favorable due to the low diffusion barrier (*31*). Otherwise, excess nucleation with random orientations will form at the typical supersaturation growth condition. The cross-sectional SEM image of GaN films is further measured to demonstrate the full growth process of GaN films (the inset of Fig. 1H). The planar GaN films have an average thickness of about 1.1 μm atop the GaN nanorods with a uniform height of about 400 nm. At the interface between the nanorods and planar film, the top of nanorods shows an inverted pyramid shape, formed during the epitaxial lateral overgrowth (ELOG) process, shown in the inset of Fig. 1H labeled by orange dotted lines.

X-ray diffraction (XRD) peaks are observed only at 34.6° and 72.9°, corresponding to the (0002) and (0004) orientations of wurtzite GaN, respectively, indicating that GaN films have a consistent out-of-plane orientation (Fig. 1I). The x-ray rocking curve full width at the half maximum (FWHM) of the (0002) peak is 1.2° (the inset of Fig. 1I). Raman spectrum of GaN films exhibits a slight red shift of E_2 (high) peak with respect to stress-free bulk GaN, showing that

small tensile stress exists in as-grown GaN films (fig. S4B). The SEM, XRD, and Raman results suggest that the Gr and vertically aligned GaN nanorod template play critical roles in modulating the lattice arrangement at the nitride/Gr interface.

Although plenty of work on vdWE have been realized, understanding of kinetic mechanism and atomic structure at the nitride/Gr interface and interpretations of variational in-plane orientations have not reached a consensus (*32*–*36*). Here, to study the interfacial properties and further identify structural models of GaN/pristine-Gr, we perform first-principles calculations based on density functional theory (DFT) using the van der Waals density functional (DF) optB86b (*37*). According to the periodicity of the hexagonal lattice, there are six kinds of possible lattice configurations for GaN and Gr, with in-plane rotation angles of 0°, 30°, 19.1°, 13.9°, 10.9°, and 23.4° (fig. S7). For the heteroepitaxy of GaN on Gr, lattice mismatch needs to be considered, resulting in the following possible epitaxial relationships of GaN/Gr: grain 1, GaN 0°//Gr 0°; grain 2, GaN 10.9°//Gr 0°; grain 3, GaN 0°//Gr 30°; grain 4, GaN 19.1°//Gr 30°; grain 5, GaN 13.9°//Gr 10.9°; grain 6, GaN 30°//Gr 10.9°; and grain 7, GaN 0°//Gr 19.1° (table. S1). With the variation of the distance at the interface between GaN and Gr, the formation energy of each alignment changes as a quadratic function (Fig. 2B). According to the Minimum Energy Principle, the most preferred grains for GaN are grain 2, grain 1, and grain 3 in the order mentioned. Specifically, the corresponding lattice configurations are GaN 10.9°//Gr 0°, GaN 0°//Gr 0°, and GaN 0°//Gr 30°, with in-plane rotation angles of 10.9°, 0°, and 30°, respectively. Moreover, the difference charge density at the heterointerface (Fig. 2A) represents a vdWE binding feature without electron orbital hybridization. The calculated binding energy of the GaN/Gr heterointerface varies from 34 to 56 meV per atom, which is a typical vdWE binding energy and similar to that of the Gr/InAs interface (*34*).

High-resolution transmission electron microscopy (HRTEM) is further used to examine the in-plane orientations of GaN grown on Gr/glass. Figure 2 (C and D) shows the grain boundaries between grain 1 and grain 2, as well as grain 1 and grain 3. Their relative misorientation angles are measured to be 10° and 29°, respectively, by the corresponding fast Fourier transform (FFT) images in the inset of Fig. 2 (C and D). In addition, the HRTEM images from each grain and the corresponding FFT images show well-ordered hexagonal atomic arrangements of wurtzite GaN with rotation angles of 0°, 10°, and 29° (Fig. 2E), which matches well with the DFT calculation

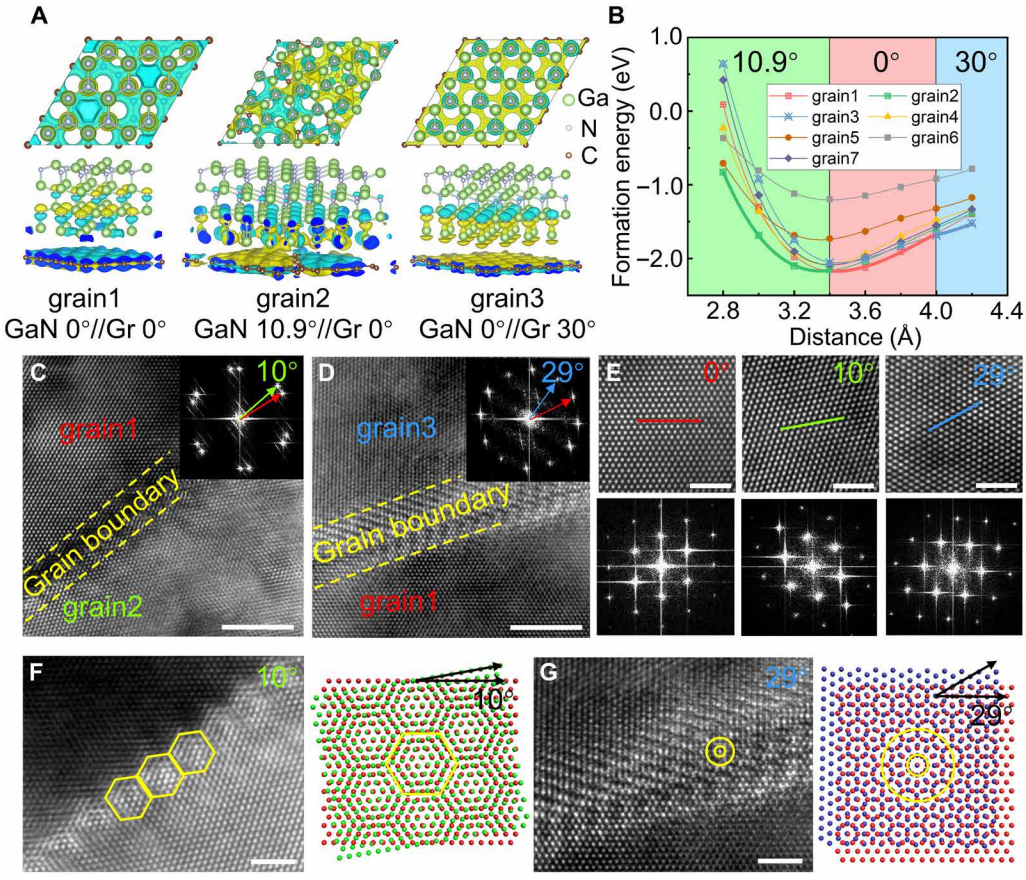

Fig. 2. The in-plane orientation of GaN grown on Gr. (**A**) Calculated models of GaN/Gr for grain 1, GaN 0°//Gr 0°, grain 2, GaN 10.9°//Gr 0°, and grain 3, GaN 0°//Gr 30°. (**B**) DFT calculations for the GaN/Gr interface showing three kinds of preferential grains of GaN films grown on Gr with rotation angles of 0°, 10.9°, and 30°. The grain boundary (**C**) between grain 1 and grain 2 and (**D**) between grain 1 and grain 3. The insets show FFT images from the boundary with the relative rotation angles of 10° and 29°, respectively. (**E**) HRTEM and corresponding FFT images from each grain showing well-ordered hexagonal atomic arrangements of wurtzite GaN. (**F** and **G**) HRTEM images and structural representations of the Moiré patterns for the overlap of two GaN layers with 10° and 29° relative rotations, respectively. Scale bars, 5 nm (C and D) and 2 nm (E to G).

results shown in Fig. 2B. Moreover, clear Moiré patterns are observed in both grain boundaries because of the overlap of two adjacent grains (Fig. 2, F and G, left). The right images in Fig. 2 (F and G) show the structural representations of the Moiré patterns formed by two layers of GaN with relative rotation angles of 10° and 29°, respectively, which agree well with the HRTEM images. The electron backscatter diffraction (EBSD) inverse pole figure (IPF) images and XRD φ scan also lead to the same conclusion (fig. S8).

We further grow the blue LED structure to verify the optical properties of GaN films grown on Gr/glass. Figure 3A shows the schematic diagram of the blue LED structure grown on coalesced GaN films with five pairs of $In_xGa_{1-x}N$/GaN multiple quantum wells (MQWs) and a p-GaN layer. From the XRD 2θ-ω scan of $In_xGa_{1-x}N$/GaN MQWs (Fig. 3D), the intense GaN (0002) peak and satellite peaks from the MQWs up to the third order are observed, indicating good periodicity and high quality of MQWs. The typical cross-sectional TEM image of the full LED structure can be found in Fig. 3B, where the fully coalesced n-GaN layer, $In_xGa_{1-x}N$/GaN MQWs, and the p-GaN layer are on top of bridging nanorods grown on a Gr/glass substrate. Figure 3C shows the HRTEM image of the nitrides/Gr/glass interface. The Gr layer is continuous and can be observed between the nucleation layer and the glass substrate, which is indicated by yellow dotted lines. In addition, a thin C element layer is observed in energy dispersive spectroscopy (EDS) mapping of Si, C, and Ga elements at the interface of nitrides/Gr/glass, verifying the existence of Gr (fig. S9). We further used *Z*-contrast high-angle annular dark-field (HAADF) scanning TEM (STEM) image (Fig. 3E) to show the five pairs of MQWs, in which the GaN barriers and $In_xGa_{1-x}N$ wells show different contrasts, dark and bright, respectively. The corresponding EDS mapping of In element indicates the uniform distribution in each layer of $In_xGa_{1-x}N$ wells (Fig. 3F). Figure 3G shows the atomic STEM image of the $In_xGa_{1-x}N$/GaN quantum well with ordered atomic arrangements with the growth direction of GaN films along [0001].

The optical characteristics of the blue LED are investigated by photoluminescence (PL). The photograph in Fig. 4A shows strong blue PL emission at room temperature. The room temperature PL spectrum in Fig. 4D shows a main peak at 477 nm, corresponding to the emission from the $In_xGa_{1-x}N$/GaN MQWs active region, and a minor peak at 365 nm related to the near–band-edge emission of GaN. Furthermore, the temperature dependence of the PL spectra from 5 to 300 K is measured to estimate the IQE of the blue LED (Fig. 4E). There is no obvious yellow luminescence band or other defect-related emissions in spectra even at low temperature (5 K), indicating the high quality and low defect density of GaN and InGaN films. Figure 4F shows the integrated PL intensity as a function of the reciprocal of temperature. The ratio of the integrated PL intensity at 300 to 5 K is 48.67%, which is commonly defined as the IQE assuming that the IQE at 5 K is equal to 100% (*38*, *39*).

The use of Gr makes it possible for the nondestructive release of epitaxial layers from brittle substrates, which is crucial for the fabrication of flexible devices (*40*–*44*). We successfully transfer the GaN-based blue LED epilayer from the glass substrate onto a conducting polymer (Fig. 4B). The flexible device emits a blue electroluminescence (EL) emission (Fig. 4C and fig. S10).

In summary, we provide a strategy for the vdWE of nitrides on amorphous substrates. Gr plus nitride nanorod buffer layer is adopted to control the orientation alignment during the MOCVD process. The obtained GaN films exhibit a nearly single-crystalline characteristic with a well-controlled lattice arrangement in both in-plane and out-of-plane orientations. The in-plane orientation and interface atomic configurations are theoretically analyzed by DFT calculations and experimentally confirmed by plan-view HRTEM and EBSD measurements. The fabricated blue LED with $In_xGa_{1-x}N$/GaN MQWs shows a record IQE (48.67%) for nitride MQW LEDs on amorphous substrates. Last, a flexible inorganic light-emitting device is demonstrated. Our work offers a practical approach to nitride semiconductor vdWE and opens a new dimension for flexible

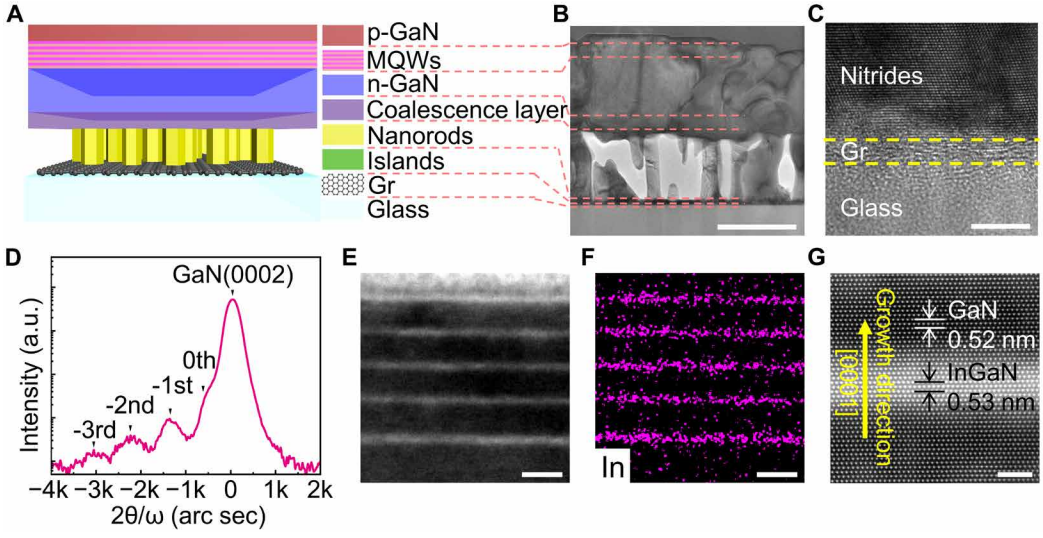

Fig. 3. The structural properties of blue LED grown on GaN/Gr/glass. (**A**) Schematic diagram of the blue LED structure. (**B**) Cross-sectional TEM image of the blue LED structure, showing vertical nanorods, consecutive n-GaN film, MQWs, and a p-GaN layer. (**C**) HRTEM image of the AlGaN/Gr/glass interface showing the presence of Gr. (**D**) XRD 2θ-ω scan of MQWs showing the good periodicity and high quality of MQWs. (**E**) Cross-sectional HAADF image of MQWs showing five pairs of GaN barriers and $In_xGa_{1-x}N$ wells. (**F**) Corresponding EDS mapping of In element showing uniform distributions within wells. (**G**) Atomic-resolution HAADF image of an $In_xGa_{1-x}N$/GaN QW lattice showing the [0001] growth direction and ordered atomic arrangements. Scale bars, 500 nm (B), 5 nm (C), 20 nm (E and F), and 2 nm (G).

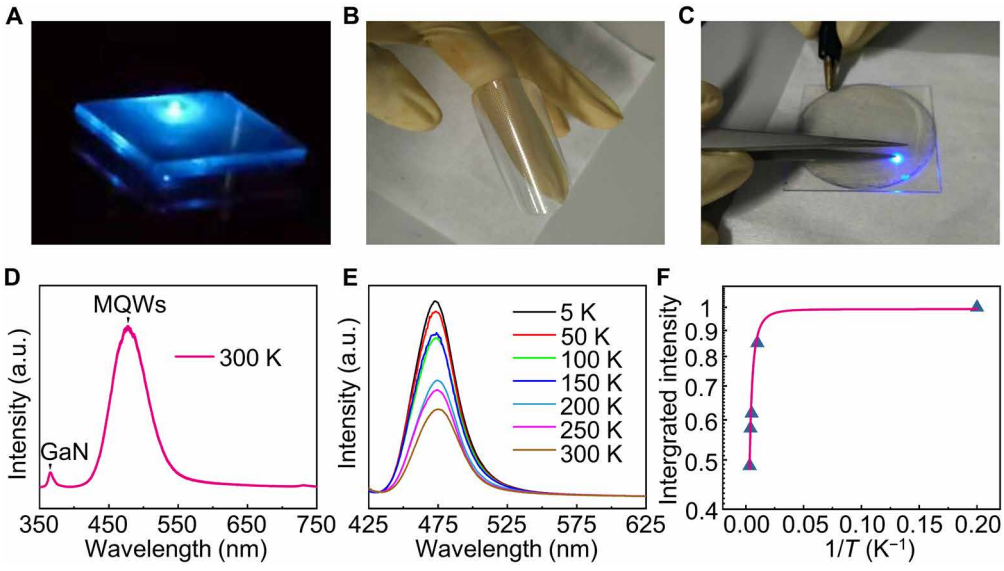

Fig. 4. The optical characteristics and transfer of blue LED grown on GaN/Gr/glass. (**A**) Photograph of the blue LED at room temperature showing strong blue luminescence. Photo credit: Fang Ren, Institute of Semiconductors, Chinese Academy of Sciences. (**B**) Photograph of flexible blue LED exfoliated from the glass substrate. Photo credit: Zhiqiang Liu, Institute of Semiconductors, Chinese Academy of Sciences. (**C**) Photograph of the blue EL emission of a flexible LED. Photo credit: Zhiqiang Liu, Institute of Semiconductors, Chinese Academy of Sciences. (**D**) Room temperature PL spectrum of blue LED showing luminescence peak of MQWs at 477 nm and luminescence peak of GaN at 365 nm. (**E**) Temperature-dependent PL spectra of blue LED showing the decrease of PL intensity with the increase of temperature. (**F**) Temperature dependence of integrated PL intensity of emissions from MQWs showing a relatively high IQE of 48.67%.

integration of diverse material systems for future electronics and photonics.

MATERIALS AND METHODS

Transfer of Gr

The Gr transferred on amorphous glass was grown on copper foil by the CVD method. During the transfer process, poly(methylmethacrylate) (PMMA) was used as a handle to reduce breakage or wrinkles on Gr. We first spin cast PMMA onto the Gr copper foil that was afterward heated at 120°C for 3 min to dry the PMMA. Then, the copper foil was etched away by 20% $FeCl_3$ solution and the PMMA/Gr film could float on the liquid surface owing to the surface tension. After washing by deionized water, the Gr was picked up by the amorphous glass and baked under an infrared lamp for 10 min to remove the liquid and make the Gr stick tightly on the glass. Last, the PMMA handler was dissolved in acetone.

Growth of nanorods on Gr/glass

Throughout the growth process, we adopted trimethylgallium (TMGa), trimethylaluminum (TMAl), and ammonia (NH_3) as precursors, and hydrogen (H_2) as the carrier gas. Before the growth of nanorods, NH_3 was introduced into the chamber of MOCVD (Aixtron, a close-coupled showerhead system) for the nitridation process with a flow of 7200 standard cubic centimeter per minute (sccm) for 150 s. Afterward, AlGaN nucleation islands were deposited for 60 s by introducing TMGa and TMAl with a flow of 50 and 162 sccm, respectively. AlGaN nanorods were subsequently grown by introducing TMGa and NH_3 with a flux of 172 and 90 sccm and decreasing TMAl flow to 54 sccm. All growth steps of nanorods were conducted at 66 mbar and 1280°C. The growth temperature in all processes refers to the set value.

ELOG and coalescence of nanorods

Following the growth of vertically aligned nanorods, the growth temperature was decreased to 1260°C, and the NH_3 flow was increased to 240 sccm to induce the ELOG of nanorods, while the TMAl flow was decreased to 35 sccm. Other growth conditions were kept constant. The ELOG process lasted for 1500 s to obtain a fully coalesced film.

Formation of flat n-GaN film

The growth temperature was increased to 1290°C, and the NH_3 flow was increased to 54,000 sccm for 3600 s. The TMAl source was closed and silane (SiH_4) was introduced as dopants to grow n-GaN film.

Control experiments

To investigate the role of Gr and nanorods in orientation regulation, we set up four control experiments. Sample 1 was GaN films grown on Gr-covered glass by the nanorod template. Sample 2 was GaN films directly grown on bare glass by the nanorod template. Sample 3 was GaN films directly grown on bare glass by the conventional LT method. Sample 4 was GaN films grown on Gr-covered glass by the conventional LT method. Sample 1 and sample 2 were grown under the same conditions as described above. Sample 3 and sample 4 were grown under the same conditions by the conventional LT method.

For the growth of sample 3 and sample 4, the AlGaN buffer layer was grown at 550°C for 75 s with a NH_3 flow of 56,000 sccm, a TMGa flow of 84 sccm, and a TMAl flow of 60 sccm. Then, the GaN layer was grown at 1080°C for 45 min with a NH_3 flow of 50,000 sccm and a TMGa flow of 388 sccm.

Growth of blue LED structure

The triethylgallium (TEGa), trimethylindium (TMIn), and NH_3 were adopted as precursors to grow $In_xGa_{1-x}N$ wells and GaN barriers.

Five periods of $In_xGa_{1-x}N$/GaN MQWs with 4/15 nm were grown at 850°/940°C. Then, a 20-nm-thick layer of p-GaN layer was deposited at 930°C by introducing magnesocene (Cp2Mg) as dopants.

Transfer of the epitaxial layer

Conducting polymer gel was spin-coated on the surface of the epitaxial layer grown on a 2-inch Gr/glass substrate with a rotation speed of 1000 rpm for 1 min and baked on the hot plate at 130°C for 15 min. Then, the solidified conducting polymer with the epitaxial layer was mechanically exfoliated from the substrate using thermal release tape. Last, the thermal release tape was released at 120°C.

Characterization

The as-grown epitaxial layer was characterized by SEM (Hitachi, Tokyo, Japan; operated at 4.4 kV), atomic force microscopy (D3100, Veeco, New York, NY, USA), XRD (Bede D1, UK; operated at 40 kV, 35 mA), Raman microscopy (Horiba, Kyoto, Japan; 532-nm laser excitation), and TEM/STEM (JEM-F200, Japan; Tecnai F20, USA; Titan Cubed Themis G2 300, USA) equipped with an EDS detector. The blue LED was characterized by PL (Horiba, Kyoto, Japan; 325-nm He-Cd laser with a power of 100 mW and cooled by liquid helium).

First-principles calculations

The first-principles calculations within DFT were performed using the Vienna Ab initio Simulation Package. We adopted the projector augmented wave pseudopotential and the generalized gradient approximation of Perdew-Burke-Ernzerhof for the exchange-correlation functional. The cutoff energy was chosen to be 350 eV, and full structural optimization was performed until atomic forces were less than 0.02 eV/Å. The van der Waals interactions were modeled by the optB88 exchange functional. The interface systems were molded using supercells containing four bilayers of nitrides and one layer of Gr. We fixed the top layer of GaN to keep the symmetry of the wurtzite structure. The vacuum region was chosen to be 10 Å.

SUPPLEMENTARY MATERIALS

Supplementary material for this article is available at http://advances.sciencemag.org/cgi/content/full/7/31/eabf5011/DC1

REFERENCES AND NOTES

1. Y. Liu, Y. Huang, X. Duan, Van der Waals integration before and beyond two-dimensional materials. *Nature* **567**, 323–333 (2019).
2. W. Kong, H. Li, K. Qiao, Y. Kim, K. Lee, Y. Nie, D. Lee, T. Osadchy, R. J. Molnar, D. K. Gaskill, R. L. Myers-Ward, K. M. Daniels, Y. Zhang, S. Sundram, Y. Yu, S.-h. Bae, S. Rajan, Y. Shao-Horn, K. Cho, A. Ougazzaden, J. C. Grossman, J. Kim, Polarity governs atomic interaction through two-dimensional materials. *Nat. Mater.* **17**, 999–1004 (2018).
3. M. Chhowalla, H. S. Shin, G. Eda, L.-J. Li, K. P. Loh, H. Zhang, The chemistry of two-dimensional layered transition metal dichalcogenide nanosheets. *Nat. Chem.* **5**, 263–275 (2013).
4. S. Garaj, W. Hubbard, A. Reina, J. Kong, D. Branton, J. A. Golovchenko, Graphene as a subnanometre trans-electrode membrane. *Nature* **467**, 190–193 (2010).
5. Z. Chen, X. Zhang, Z. Dou, T. Wei, Z. Liu, Y. Qi, H. Ci, Y. Wang, Y. Li, H. Chang, J. Yan, S. Yang, Y. Zhang, J. Wang, P. Gao, J. Li, Z. Liu, High-brightness blue light-emitting diodes enabled by a directly grown graphene buffer layer. *Adv. Mater.* **30**, 1801608 (2018).
6. H. Chang, Z. Chen, W. Li, J. Yan, R. Hou, S. Yang, Z. Liu, G. Yuan, J. Wang, J. Li, P. Gao, T. Wei, Graphene-assisted quasi-van der Waals epitaxy of AlN film for ultraviolet light emitting diodes on nano-patterned sapphire substrate. *Appl. Phys. Lett.* **114**, 091107 (2019).
7. T. H. Seo, A. H. Park, S. Park, Y. H. Kim, G. H. Lee, M. J. Kim, M. S. Jeong, Y. H. Lee, Y.-B. Hahn, E.-K. Suh, Direct growth of GaN layer on carbon nanotube-graphene hybrid structure and its application for light emitting diodes. *Sci. Rep.* **5**, 7747 (2015).
8. J.-K. Choi, J.-H. Huh, S.-D. Kim, D. Moon, D. Yoon, K. Joo, J. Kwak, J. H. Chu, S. Y. Kim, K. Park, Y.-W. Kim, E. Yoon, H. Cheong, S.-Y. Kwon, One-step graphene coating of heteroepitaxial GaN films. *Nanotechnology* **23**, 435603 (2012).
9. Y. Qi, Y. Wang, Z. Pang, Z. Dou, T. Wei, P. Gao, S. Zhang, X. Xu, Z. Chang, B. Deng, S. Chen, Z. Chen, H. Ci, R. Wang, F. Zhao, J. Yan, X. Yi, K. Liu, H. Peng, Z. Liu, L. Tong, J. Zhang, Y. Wei, J. Li, Z. Liu, Fast growth of strain-free AlN on graphene-buffered sapphire. *J. Am. Chem. Soc.* **140**, 11935–11941 (2018).
10. L. Fan, X. Sun, C. Xiong, C. Schuck, H. X. Tang, Aluminum nitride piezo-acousto-photonic crystal nanocavity with high quality factors. *Appl. Phys. Lett.* **102**, 153507 (2013).
11. M. Heilmann, A. M. Munshi, G. Sarau, M. Goebelt, C. Tessarek, V. T. Fauske, A. T. J. van Helvoort, J. Yang, M. Latzel, B. Hoffmann, G. Conibeer, H. Weman, S. Christiansen, Vertically oriented growth of GaN nanorods on Si using graphene as an atomically thin buffer layer. *Nano Lett.* **16**, 3524–3532 (2016).
12. F. Ren, Y. Yin, Y. Wang, Z. Liu, M. Liang, H. Ou, J. Ao, T. Wei, J. Yan, G. Yuan, X. Yi, J. Wang, J. Li, D. Dasa, H. Weman, Direct growth of AlGaN nanorod LEDs on graphene-covered Si. *Materials* **11**, 2372 (2018).
13. Y. Wang, D. Dheeraj, Z. Liu, M. Liang, Y. Li, X. Yi, J. Wang, J. Li, H. Weman, AlGaN nanowires grown on SiO_2/Si (100) using graphene as a buffer layer. *Cryst. Growth Des.* **19**, 5516–5522 (2019).
14. Y. Feng, X. Yang, Z. Zhang, D. Kong, J. Zhang, K. Liu, X. Li, J. Shen, F. Liu, T. Wang, P. Ji, F. Xu, N. Tang, T. Yu, X. Wang, D. Yu, W. Ge, B. Shen, Epitaxy of single-crystalline GaN film on CMOS-compatible Si(100) substrate buffered by graphene. *Adv. Funct. Mater.* **29**, 1905056 (2019).
15. Y. Wang, S. Yang, H. Chang, W. Li, X. Chen, R. Hou, J. Yan, X. Yi, J. Wang, T. Wei, Flexible graphene-assisted van der Waals epitaxy growth of crack-free AlN epilayer on SiC by lattice engineering. *Appl. Surf. Sci.* **520**, 146358 (2020).
16. N. Nepal, V. D. Wheeler, T. J. Anderson, F. J. Kub, M. A. Mastro, R. L. Myers-Ward, S. B. Qadri, J. A. Freitas, S. C. Hernandez, L. O. Nyakiti, S. G. Walton, K. Gaskill, C. R. Eddy Jr., Epitaxial growth of III-nitride/graphene heterostructures for electronic devices. *Appl. Phys. Express* **6**, 061003 (2013).
17. S. Fernandez-Garrido, M. Ramsteiner, G. Gao, L. A. Galves, B. Sharma, P. Corfdir, G. Calabrese, Z. De Souza Schiaber, C. Pfueller, A. Trampert, J. M. J. Lopes, O. Brandt, L. Geelhaar, Molecular beam epitaxy of GaN nanowires on epitaxial graphene. *Nano Lett.* **17**, 5213–5221 (2017).
18. R. Yan, G. Khalsa, S. Vishwanath, Y. H. An, J. Wright, S. R. Ouvimov, D. S. Katzer, N. Nepal, B. P. Downey, D. A. Muller, H. G. Xing, D. J. Meyer, D. Jena, GaN/NbN epitaxial semiconductor/superconductor heterostructures. *Nature* **555**, 183–189 (2018).
19. Y. Kim, S. S. Cruz, K. Lee, B. O. Alawode, C. Choi, Y. Song, J. M. Johnson, C. Heidelberger, W. Kong, S. Choi, K. Qiao, I. Almansouri, E. A. Fitzgerald, J. Kong, A. M. Kolpak, J. Hwang, J. Kim, Remote epitaxy through graphene enables two-dimensional material-based layer transfer. *Nature* **544**, 340–343 (2017).
20. K. Chen, R. Kapadia, A. Harker, S. Desai, J. S. Kang, S. Chuang, M. Tosun, C. M. Sutter-Fella, M. Tsang, Y. Zeng, D. Kiriya, J. Hazra, S. R. Madhvapathy, M. Hettick, Y.-Z. Chen, J. Mastandrea, M. Amani, S. Cabrini, Y.-L. Chueh, J. W. Ager III, D. C. Chrzan, A. Javey, Direct growth of single-crystalline III-V semiconductors on amorphous substrates. *Nat. Commun.* **7**, 10502 (2016).
21. J. H. Choi, A. Zoulkarneev, S. I. Kim, C. W. Baik, M. H. Yang, S. S. Park, H. Suh, U. J. Kim, H. Bin Son, J. S. Lee, M. Kim, J. M. Kim, K. Kim, Nearly single-crystalline GaN light-emitting diodes on amorphous glass substrates. *Nat. Photonics* **5**, 763–769 (2011).
22. J. H. Choi, H. Y. Ahn, Y. S. Lee, K. Park, T.-H. Kim, K. S. Cho, C. W. Baik, S. I. Kim, H. Yoo, E. H. Lee, B. L. Choi, S.-D. Kim, Y.-W. Kim, M. Kim, S. Hwang, GaN light-emitting diodes on glass substrates with enhanced electroluminescence. *J. Mater. Chem.* **22**, 22942–22948 (2012).
23. A. Prabaswara, J.-W. Min, C. Zhao, B. Janjua, D. Zhang, A. M. Albadri, A. Y. Alyamani, T. K. Ng, B. S. Ooi, Direct growth of III-nitride nanowire-based yellow light-emitting diode on amorphous quartz using thin Ti interlayer. *Nanoscale Res. Lett.* **13**, 41 (2018).
24. I. M. Hoiaas, A. Liudi Mulyo, P. E. Vullum, D.-C. Kim, L. Ahtapodov, B.-O. Fimland, K. Kishino, H. Weman, GaN/AlGaN nanocolumn ultraviolet light-emitting diode using double-layer graphene as substrate and transparent electrode. *Nano Lett.* **19**, 1649–1658 (2019).
25. A. Liudi Mulyo, M. K. Rajpalke, H. Kuroe, P.-E. Vullum, H. Weman, B.-O. Fimland, K. Kishino, Vertical GaN nanocolumns grown on graphene intermediated with a thin AlN buffer layer. *Nanotechnology* **30**, 015604 (2019).
26. J. W. Shon, J. Ohta, K. Ueno, A. Kobayashi, H. Fujioka, Fabrication of full-color InGaN-based light-emitting diodes on amorphous substrates by pulsed sputtering. *Sci. Rep.* **4**, 5325 (2014).
27. J. Yu, J. Wang, W. Yu, C. Wu, B. Lu, J. Deng, Z. Zhang, X. Li, Z. Hao, L. Wang, Y. Han, Y. Luo, C. Sun, B. Xiong, H. Li, Low-temperature and global epitaxy of GaN on amorphous glass substrates by molecular beam epitaxy via a compound buffer layer. *Thin Solid Films* **662**, 174–179 (2018).
28. S. Ozen, Zr-doped GaN thin films grown onto glass and PET substrates by thermionic vacuum arc. *Mater. Res. Express* **6**, 046401 (2019).
29. J. Nomoto, T. Tsuchiya, T. Yamamoto, Well-defined (0001)-oriented aluminum nitride polycrystalline films on amorphous glass substrates deposited by ion plating with direct-current arc discharge. *Appl. Surf. Sci.* **478**, 998–1003 (2019).

30. M. Hainey Jr., Y. Robin, G. Avit, H. Amano, N. Usami, Scalable fabrication of GaN on amorphous substrates via MOCVD on highly oriented silicon seed layers. *J. Cryst. Growth* **535**, 125522 (2020).
31. K. T. Chan, J. B. Neaton, M. L. Cohen, First-principles study of metal adatom adsorption on graphene. *Phys. Rev. B* **77**, 235430 (2008).
32. A. M. Munshi, D. L. Dheeraj, V. T. Fauske, D.-C. Kim, A. T. J. van Helvoort, B.-O. Fimland, H. Weman, Vertically aligned GaAs nanowires on graphite and few-layer graphene: Generic model and epitaxial growth. *Nano Lett.* **12**, 4570–4576 (2012).
33. A. M. Munshi, H. Weman, Advances in semiconductor nanowire growth on graphene. *Phys. Status Solidi* **7**, 713–726 (2013).
34. Y. J. Hong, J. W. Yang, W. H. Lee, R. S. Ruoff, K. S. Kim, T. Fukui, Van der Waals epitaxial double heterostructure: InAs/single-layer graphene/InAs. *Adv. Mater.* **25**, 6847–6853 (2013).
35. V. Kumaresan, L. Largeau, A. Madouri, F. Glas, H. Zhang, F. Oehler, A. Cavanna, A. Babichev, L. Travers, N. Gogneau, M. Tchernycheva, J.-C. Harmand, Epitaxy of GaN nanowires on graphene. *Nano Lett.* **16**, 4895–4902 (2016).
36. H. Yoo, S. Yoon, K. Chung, S.-H. Kang, Y.-K. Kwon, G.-C. Yi, M. Kim, Understanding luminescence properties of grain boundaries in GaN thin films and their atomistic origin. *Appl. Phys. Lett.* **112**, 131901 (2018).
37. G. Feldbauer, M. Wolloch, P. O. Bedolla, P. Mohn, J. Redinger, A. Vernes, Adhesion and material transfer between contacting Al and TiN surfaces from first principles. *Phy. Rev. B* **91**, 165413 (2015).
38. X. Liu, B. H. Le, S. Y. Woo, S. Zhao, A. Pofelski, G. A. Botton, Z. Mi, Selective area epitaxy of AlGaN nanowire arrays across nearly the entire compositional range for deep ultraviolet photonics. *Opt. Express* **25**, 30494–30502 (2017).
39. J. Mickevicius, G. Tamulaitis, M. Shur, M. Shatalov, J. Yang, R. Gaska, Internal quantum efficiency in AlGaN with strong carrier localization. *Appl. Phys. Lett.* **101**, 211902 (2012).
40. J. Yu, L. Wang, Z. Hao, Y. Luo, C. Sun, J. Wang, Y. Han, B. Xiong, H. Li, Van der Waals epitaxy of III-nitride semiconductors based on 2D materials for flexible applications. *Adv. Mater.* **32**, 1903407 (2020).
41. Y. Kobayashi, K. Kumakura, T. Akasaka, T. Makimoto, Layered boron nitride as a release layer for mechanical transfer of GaN-based devices. *Nature* **484**, 223–227 (2012).
42. J. Kim, C. Bayram, H. Park, C.-W. Cheng, C. Dimitrakopoulos, J. A. Ott, K. B. Reuter, S. W. Bedell, D. K. Sadana, Principle of direct van der Waals epitaxy of single-crystalline films on epitaxial graphene. *Nat. Commun.* **5**, 4836 (2014).
43. K. Chung, C.-H. Lee, G.-C. Yi, Transferable GaN layers grown on ZnO-coated graphene layers for optoelectronic devices. *Science* **330**, 655–657 (2010).
44. Y. Jia, J. Ning, J. Zhang, C. Yan, B. Wang, Y. Zhang, J. Zhu, X. Shen, J. Dong, D. Wang, Y. Hao, Transferable GaN enabled by selective nucleation of AlN on graphene for high-brightness violet light-emitting diodes. *Adv. Opt. Mater.* **8**, 1901632 (2020).

Acknowledgments

Funding: This research was funded by the National Key Research and Development Program of China (grant nos. 2019YFA0708202, 2016YFB0400102, and 2017YFB0403101), the National Natural Science Foundation of China (61974140, 61604140, and 11974023), and the Youth Supporting Program of Institute of Semiconductors. **Author contributions:** Zhiqiang Liu, P.G., and Zhongfan Liu conceived the idea. F.R., Y.Y., and M.L. designed and performed the growth experiments. Bingyao Liu, Z.C., J.S., B.J., and Bingzhi Liu contributed to the growth and transfer of graphene. G.Y., J.Y., T.W., and X.Y. contributed to the measurements and analyses of epilayer. Bingyao Liu, S.Z., and Zhetong Liu carried out the TEM/STEM characterizations and analyses. Jianwei Wang and Zhiqiang Liu carried out the DFT calculations. Junxi Wang and J.L. carried out the transfer of epilayer. F.R., Bingyao Liu, Z.C., Y.Z., P.G., Zhongfan Liu, and Zhiqiang Liu contributed to the schematics and photographs and cowrote the manuscript. All authors discussed the results and commented on the manuscript. **Competing interests:** The authors declare that they have no competing interests. **Data and materials availability:** All data needed to evaluate the conclusions in the paper are present in the paper and/or the Supplementary Materials.

Submitted 30 October 2020
Accepted 15 June 2021
Published 30 July 2021
10.1126/sciadv.abf5011

Citation: F. Ren, B. Liu, Z. Chen, Y. Yin, J. Sun, S. Zhang, B. Jiang, B. Liu, Z. Liu, J. Wang, M. Liang, G. Yuan, J. Yan, T. Wei, X. Yi, J. Wang, Y. Zhang, J. Li, P. Gao, Z. Liu, Z. Liu, Van der Waals epitaxy of nearly single-crystalline nitride films on amorphous graphene-glass wafer. *Sci. Adv.* **7**, eabf5011 (2021).

Van der Waals epitaxy of nearly single-crystalline nitride films on amorphous graphene-glass wafer

Fang Ren, Bingyao Liu, Zhaolong Chen, Yue Yin, Jingyu Sun, Shuo Zhang, Bei Jiang, Bingzhi Liu, Zhetong Liu, Jianwei Wang, Meng Liang, Guodong Yuan, Jianchang Yan, Tongbo Wei, Xiaoyan Yi, Junxi Wang, Yong Zhang, Jinmin Li, Peng Gao, Zhongfan Liu and Zhiqiang Liu

Sci Adv **7** (31), eabf5011.
DOI: 10.1126/sciadv.abf5011